iScience

CellPress
OPEN ACCESS

Article

Procr-expressing granulosa cells are highly proliferative and are important for follicle development

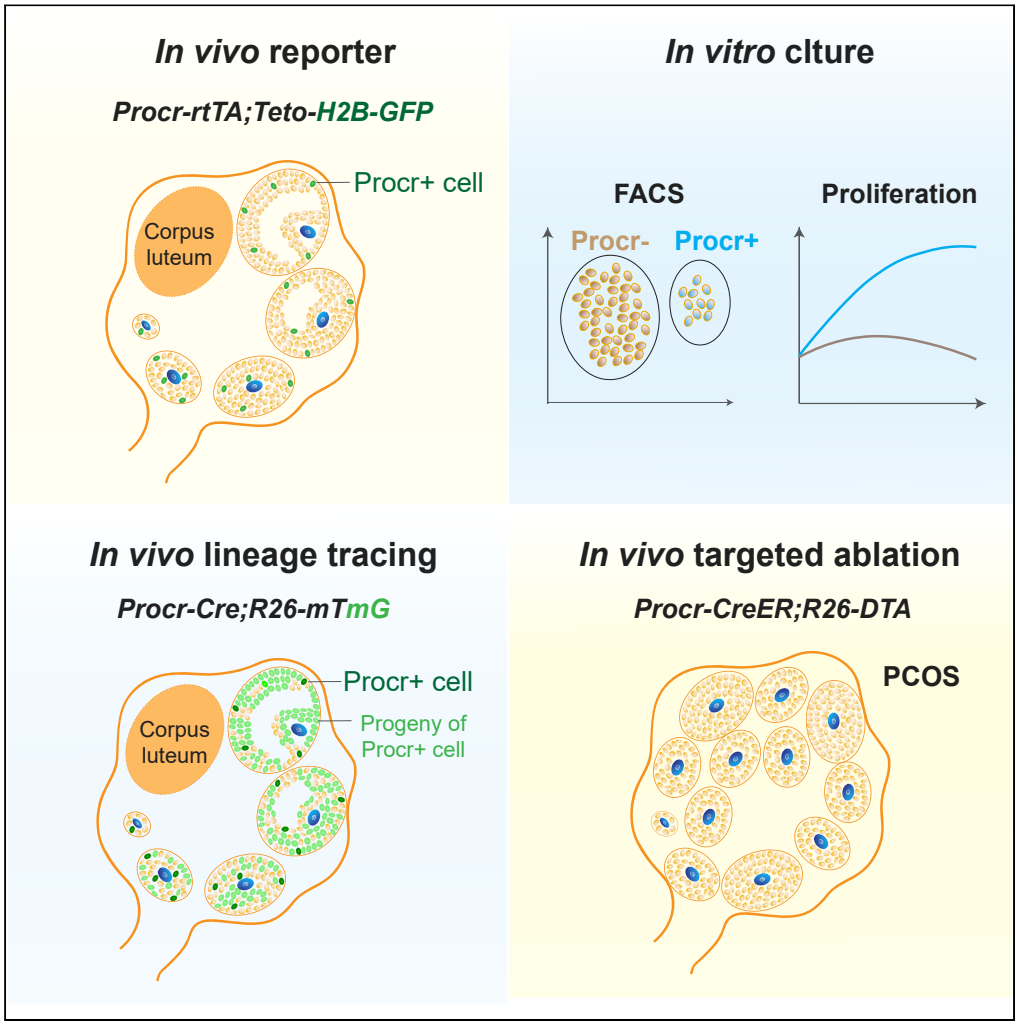

Jingqiang Wang, Kun Chu, Yinghua Wang, Jinsong Li, Junfen Fu, Yi Arial Zeng, Wen Li

fjf68@zju.edu.cn (J.F.)
yzeng@sibcb.ac.cn (Y.A.Z.)
liwen@smmu.edu.cn (W.L.)

HIGHLIGHTS

Develop a new FACS isolation method for mouse GCs

Procr marks a subset of GCs that have higher proliferative capacity

Procr+ cells contribute to increasing numbers of GCs during follicle development

Generate a PCOS mouse model with targeted ablation of Procr+ cells

Wang et al., iScience 24, 102065
February 19, 2021
https://doi.org/10.1016/j.isci.2021.102065

iScience

CellPress
OPEN ACCESS

Article

Procr-expressing granulosa cells are highly proliferative and are important for follicle development

Jingqiang Wang,[2,3,6] Kun Chu,[4,6] Yinghua Wang,[2] Jinsong Li,[2,5] Junfen Fu,[3,*] Yi Arial Zeng,[2,5,*] and Wen Li[1,7,*]

SUMMARY

Granulosa cells (GCs) play a critical role in folliculogenesis. It remains unclear how GCs expand during follicle development and whether there is a subpopulation of cells that is responsible for GCs growth. Here, we observed that a small population of GCs expressed stem cell surface marker Procr (Protein C receptor). Procr GCs displayed higher proliferation ability and lower levels of hormone receptors compared with Procr- GCs. Knockdown of Procr inhibited proliferation. Lineage tracing experiments demonstrated that they contribute to increasing numbers of GCs during folliculogenesis. Targeted ablation of Procr+ cells disrupted ovarian follicle development, leading to phenotypes of polycystic ovary syndrome. Our findings suggest that Procr-expressing GCs are endowed with high proliferative capacity that is critical for follicle development.

INTRODUCTION

Follicles are the basic functional units of the ovary, composed of an immature oocyte, surrounded by granulosa cells (GCs) and theca cells. Reproduction requires controlled development of the oocyte and the somatic cells. Once a follicle is activated, the single layer of flattened GCs first proliferate and differentiate into cuboidal GCs, awakening the dormant oocyte (Zhang and Liu, 2015; Zhang et al., 2014). In the growing follicles, GCs divide for at least 10 times to support follicle growth and oocyte maturation, reaching a total amount of over 2,000 cells at the mature antral stage (Hirshfield, 1991). At the pre-ovulatory stage, the well-differentiated GCs also provide the hormones and other factors to ensure successful ovulation (Stocco et al., 2007). Despite the significant progress made in the regulation of folliculogenesis, it remains unclear how GCs expand during follicle development and whether there is a subpopulation of cells that is responsible for GCs growth.

GCs play a critical role in folliculogenesis through their direct communication with oocytes and theca cells as well as their ability to produce and respond to hormones. Deletion of Forkhead box L2 (*Foxl2*), a key transcription factor for the development of GCs, results in mammalian ovarian failure by pervasive blockage of follicle development (Pisarska et al., 2004; Uda et al., 2004). GC-specific knockout of *Pten* gene, the negative regulator of PI3K pathway, leads to enhanced proliferation of GCs, ovulation, and the formation of corpus luteum (Fan et al., 2008). Expansion of GCs is regulated by various ovarian factors via different molecular mechanisms (Lu, 2005). For example, GDF-9 and BMP-15 secreted by oocyte are essential for GCs' proliferation in early follicular development (Eppig, 2001; Su et al., 2004). Follicle-stimulating hormone (FSH) promotes GCs' proliferation by increasing proliferating cell nuclear antigen expression and activating ERK1/2 signal pathway (Yu et al., 2005). Nerve growth factor promotes GCs' expansion by inhibiting ESR2-mediated down-regulation of CDKN1A (Wang et al., 2015b). Wnt2 acts through beta-catenin to regulate mouse GCs' proliferation (Wang et al., 2010).

Dysregulation of GC is involved in a great number of ovarian pathologies. Polycystic ovary syndrome (PCOS), the most common reproductive disorder in women of reproductive age, affects about 5%–20% of the population (Azziz et al., 2016). It is characterized by hyperandrogenism, polycystic ovarian morphology, chronic anovulation, and metabolic disorders including insulin resistance and dyslipidemia (Azziz et al., 2016; Rotterdam ESHRE/ASRM-Sponsored PCOS consensus workshop group, 2004). Because of the complicated clinical manifestations and the insufficient research models of PCOS, its pathogenesis is largely unknown and remains to be elucidated.

[1]Center of reproductive medicine, Shanghai Key Laboratory of Embryo Original Diseases, International Peace Maternity and Child Health Hospital, School of Medicine, Shanghai Jiao Tong University, Shanghai, 200030, China

[2]State Key Laboratory of Cell Biology, CAS Center for Excellence in Molecular Cell Science, Institute of Biochemistry and Cell Biology, Chinese Academy of Sciences, University of Chinese Academy of Sciences, Shanghai, 200031, China

[3]Children's Hospital, Zhejiang University School of Medicine, National Clinical Research Center for Child Health, National Children's Regional Medical Center, Hangzhou, 310052, China

[4]Reproductive Medicine Center, Changzheng Hospital, Second Military Medical University, Shanghai, 200003, China

[5]School of Life Science, Hangzhou Institute for Advanced Study, University of Chinese Academy of Sciences, Chinese Academy of Sciences, Hangzhou, 310024, China

[6]These authors contributed equally

[7]Lead contact

*Correspondence: fjf68@zju.edu.cn (J.F.), yzeng@sibcb.ac.cn (Y.A.Z.), liwen@smmu.edu.cn (W.L.)

https://doi.org/10.1016/j.isci.2021.102065

Protein C receptor (Procr) marks adult stem/progenitor cells in various tissues, including the mammary gland (Wang et al., 2015a), vascular endothelial cells (Yu et al., 2016), pancreatic islet (Wang et al., 2020), ovarian surface epithelium (OSE) (Wang et al., 2019), and hematopoietic system (Balazs et al., 2006). Procr encodes a single-pass transmembrane protein (Fukudome and Esmon, 1994). Procr expression is positively regulated by Wnt signaling (Wang et al., 2015a). Upon binding to its ligand Protein C, Procr activates several intracellular signaling, resulting in increased proliferation and survival in various tissues (Cheng et al., 2003; Gramling et al., 2010; Wang et al., 2018). Indeed, Procr+ OSE cells proliferate faster than Procr- OSE cells (Wang et al., 2019) and Procr+ endothelial cells exhibited more robust proliferation than Procr- endothelial cells (Yu et al., 2016).

In this study, we investigate the role of Procr+ GCs in folliculogenesis. We utilized Procr reporter mice and RNA *in situ* hybridization to analyze Procr expression during follicle development. We developed new protocol to isolate primary GCs and compare the proliferative abilities between Procr+ and Procr- GCs. Furthermore, through *in vivo* genetic lineage tracing and targeted ablation, we examine the contribution and significance of Procr+ GCs during follicle development.

RESULTS

Procr is expressed in a subpopulation of granulosa cells

To analyze the expression of Procr in the ovarian follicle, we utilized *Procr-rtTA;TetO-H2B-GFP* mice (Figure S1A) (Wang et al., 2019). Mice at postnatal day 10 were fed with doxycycline (Dox), and the ovaries were harvested 2 days later (Figure 1A). Shown by immunostaining of ovarian sections, Procr-expressing (GFP+) cells were detected in a small population of GCs in the follicles of different stages (Figure 1B). RNA *in situ* hybridization further validated the expression of *Procr* in developing ovarian follicles. *Procr* was detected in a small number of GCs in all follicular development stages, including primordial, primary, secondary, antral, and pre-ovulatory follicles (Figures 1C–1G). In primordial follicle, where GCs are flattened (Da Silva-Buttkus et al., 2008), Procr was readily detected in one of the GCs in the cross section of primordial follicle (Figure 1C). Quantification indicated that the percentage of Procr+ GC gradually declined to 12.42% $\pm$ 2.63% in primary follicle, 4.14% $\pm$ 0.31% in secondary follicle, 1.63% $\pm$ 0.08% in antral follicle, and 1.13% $\pm$ 0.04% in pre-ovulatory follicle (Figure 1H). This may imply that Procr+ cells exert their function in earlier stage of follicle development.

Procr+ granulosa cells have higher proliferation ability and lower differentiation level than Procr- granulosa cells

To examine the behavior of Procr+ GCs, we seek to isolate live Procr+ GCs taking advantage that Procr is a surface protein. However, the purification of GCs from ovarian cells by fluorescence-activated cell sorting (FACS) has not been successfully attempted. In previous methods, GCs were enriched by either puncture of large follicles (ignore the smaller follicles) (Kipp et al., 2007) or simply a digestion of the whole ovary of 10-day old mice (Parvari et al., 2016). Neither ways harvest complete or pure GC cells. Interestingly, we observed that in *R26-mTmG* mice, the mTomato (mTom) fluorescence is dimmer in follicles compared with the rest of the ovarian section (Figure 2A). It is unclear why an R26-driven exogenous gene would have lower expression in follicles, i.e., GCs. Nevertheless, we exploited this feature to separate GCs from the rest of ovarian cells. Dissociated ovarian cells were separated based on mTom-low and mTom-high (Figure 2B). qPCR analysis indicated that mTom-low ovarian cells, compared with the mTom-high cells, have higher expression of GC markers, such as *Cyp19a1*, *Foxl2*, *Esr2*, *Fshr*, and lower expression of theca cells marker *Esr1* (Figure 2C). These results suggest that using a R26-driven fluorescent reporter, GCs can be FACS-isolated.

Next, we further separated GCs by surface Procr expression. FACS analysis indicated that Procr+ cells comprised 1.03% $\pm$ 0.21% of total GCs (Figure 2B), in line with the observations with GFP reporter mice and RNA *in situ* results. To investigate the proliferation ability, Procr+ and Procr- GCs were placed in culture and treated with EdU for 2 hours followed by detection of fluorescence. EdU staining indicated that Procr+ GCs have significantly higher proliferative ability than Procr- GCs (Figures 2D and 2E). This was further examined in isolated primary cell culture. Same amount of Procr+ and Procr- GCs were plated in culture, and cell numbers were counted during serial passages. Consistent with the *in vivo* results, Procr+ GCs in culture also proliferate faster than Procr- GCs (Figures 2E–2G).

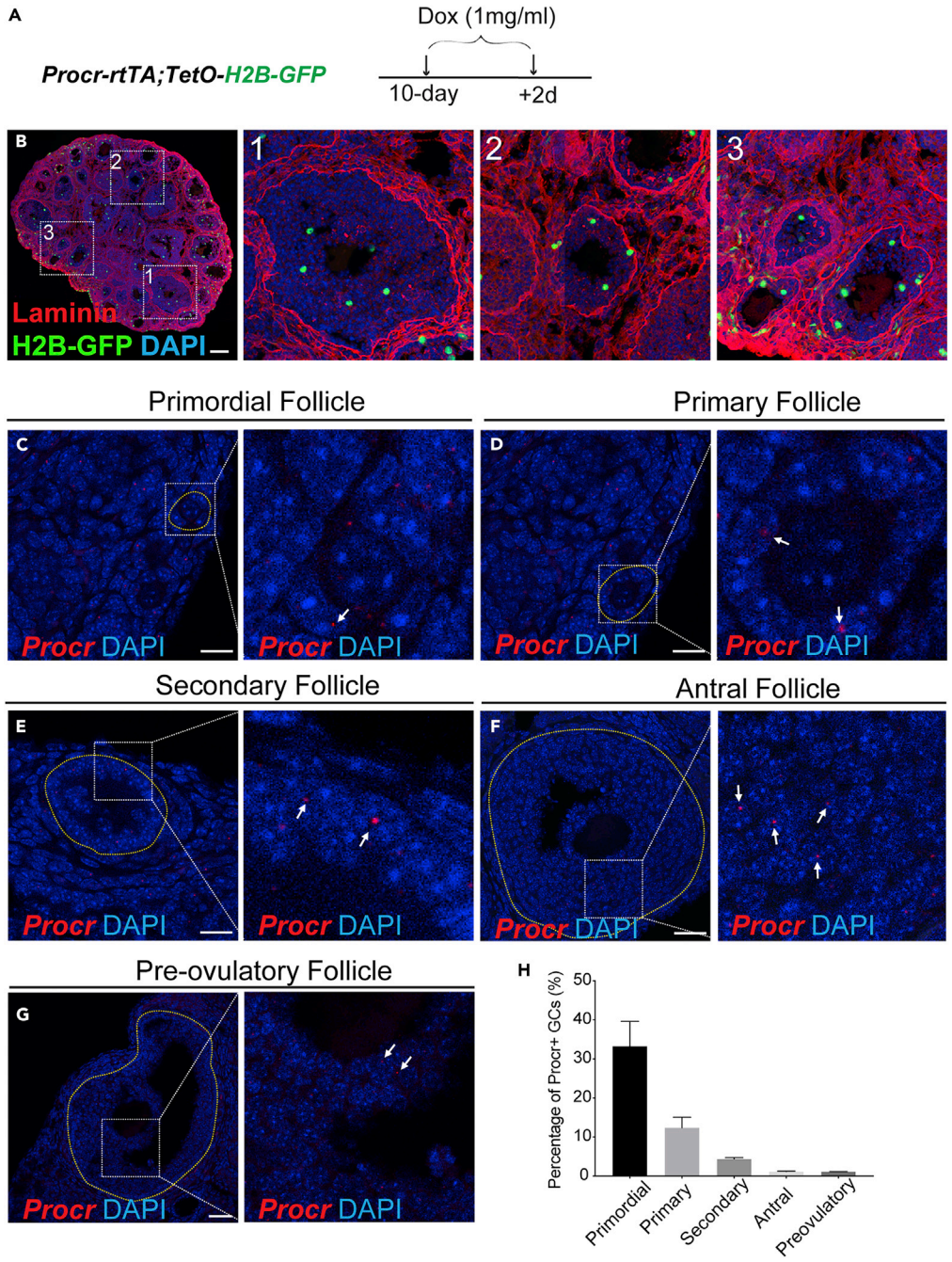

Figure 1. Procr is expressed in a subpopulation of granulosa cells

(A and B) *Procr-rtTA;TetO-H2B-GFP* mice at postnatal day 10 were fed with doxycycline for 2 days to induce the expression of H2B-GFP protein in Procr+ cells (A). Confocal images of an ovary section exhibited H2B-GFP expression in the ovarian follicles (B). Scale bar, 100 μm. n = 3 mice and representative image was shown.

(C–H) *In situ* hybridization showing *Procr* mRNA expression in the GCs of primordial (C), primary (D), secondary (E), antral (F), and pre-ovulatory (G) follicles. Scale bars, 20 μm (C–E) and 50 μm (F and G). n = 3 mice and representative image was shown. Quantification showing the percentage of Procr+ GCs in different follicle stages (H); at least 10 follicles in different stages were counted, and data are presented as mean ± SEM.

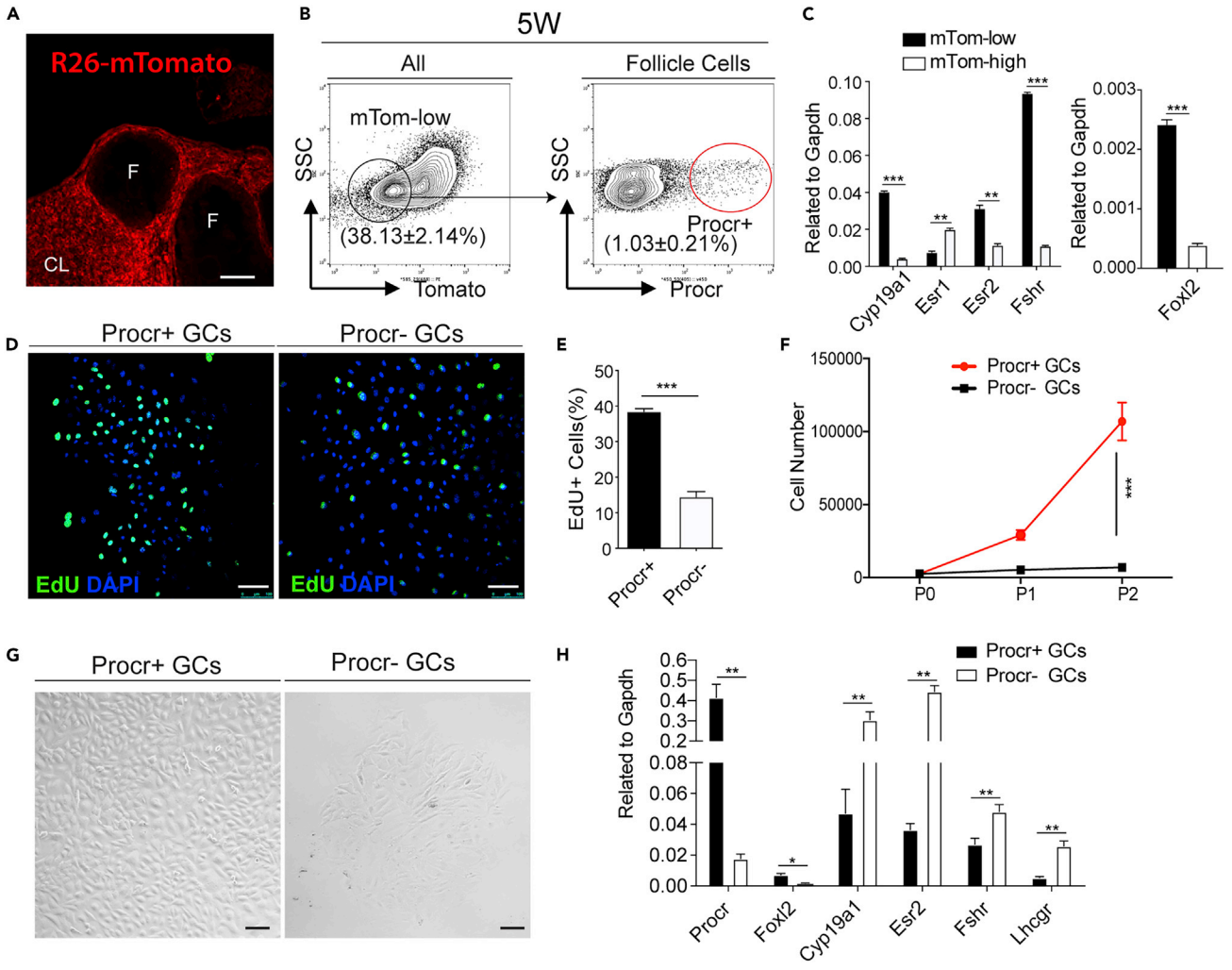

Figure 2. Procr+ granulosa cells display higher proliferation ability

(A) Section imaging of *R26-mTmG* mice ovary showing lower level of mTomato expression in GCs compared with non-GCs. Scale bar, 20 μm. F, follicle; CL, corpus luteum. n = 3 mice, and representative image was shown.

(B) FACS isolation of *R26-mTmG* ovarian cells with mTomato and Procr. The percentages of total granulosa cells (mTom-low) and Procr+ granulosa cells (mTom-low, Procr+) are as indicated. Data are pooled from three independent experiments and presented as mean ± SEM.

(C) qPCR analysis of *Cyp19a1*, *Foxl2*, *Esr1*, *Esr2*, and *Fshr* in isolated mTom-low and mTom-high ovarian cells verifying the granulosa cells' property of mTom-low. n = 3, and data are presented as mean ± SEM. Unpaired two-tailed Student's t test is used for comparison. ***p < 0.001, **p < 0.01.

(D and E) Confocal imaging (D) and quantification (E) of EdU staining showing higher proliferation ability in Procr+ GCs compared with Procr- GCs. Scale bars, 100 μm. Total 317 Procr+ cells and 294 Procr- cells from three mice were counted, and data are presented as mean ± SEM. Unpaired two-tailed Student's t test is used for comparison. ***p < 0.001.

(F and G) Isolated primary Procr+ GCs and Procr- GCs were cultured, and cell numbers were counted in each passage (F). Representative images were shown (G). The growth curve showing that Procr+ GCs are more proliferative compared with Procr- GCs. n = 3 times, and data are presented as mean ± SEM. Unpaired two-tailed Student's t test is used for comparison. ***p < 0.001. Scale bars, 100 μm.

(H) qPCR analysis of *Foxl2*, *Cyp19a1*, *Fshr*, and *Lhcgr* using freshly isolated Procr+ and Procr- GCs. n = 3, and data are presented as mean ± SEM. Unpaired two-tailed Student's t test is used for comparison. **p < 0.01, *p < 0.05.

Mature GCs have the capacity of steroidogenesis. Previous studies have found that genes encoding steroidogenic enzymes (such as *Cyp19a1*) and genes encoding hormone receptors (such as *Esr*, *Fshr*, and *Lhcgr*) were upregulated during folliculogenesis (Richards and Pangas, 2010; Zhang et al., 2018), whereas an important transcription factor *Foxl2* was decreased in GCs along follicles development (Liu et al., 2015). Next we asked whether Prcor+ and Procr- GCs are different in these aspects. qPCR analysis revealed that Procr+ GCs expressed higher level of *Foxl2* and lower levels of *Cyp19a1*, *Esr2*, *Fshr*, and *Lhcgr* than Procr- GCs (Figure 2H). This may reflect an immature state of Procr+ GCs. Taken together, these results suggest

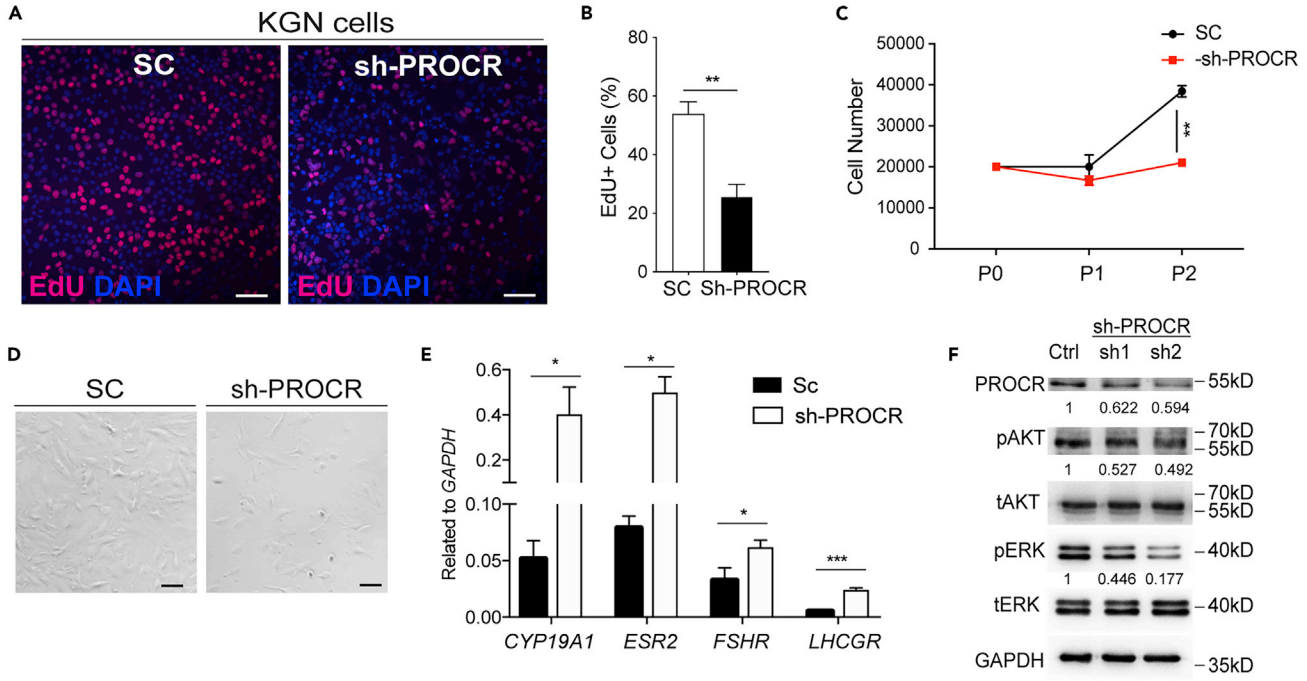

Figure 3. Knockdown of *PROCR* inhibits AKT and ERK signaling activities in granulosa cells

(A and B) Confocal imaging in KGN cells (A) and quantification (B) showing fewer EdU+ cells in sh-*PROCR* group compared with the scramble (SC). Scale bars, 100 μm. Representative image was shown. Total 1,087 KGN SC cells and 976 sh-*PROCR* cells from three different experiments were counted. Data are presented as mean ± SEM. Unpaired two-tailed Student's t test is used for comparison. $^{**}p < 0.01$.

(C and D) Cell numbers were counted in first three passages (C), and representative images (D) of KGN cells infected by scramble and *PROCR* shRNA. n = 3 times and data are presented as mean ± SEM. Unpaired two-tailed Student's t test is used for comparison. $^{**}p < 0.01$. Scale bars, 50 μm.

(E) qPCR analysis showing increased *CYP19A1*, *ESR2*, *FSHR*, and *LHCGR* with *PROCR* knockdown. n = 3 times, and data are presented as mean ± SEM. Unpaired two-tailed Student's t test is used for comparison. $^{***}p < 0.001$, $^{*}p < 0.05$.

(F) Western blots showing the decreased p-AKT and p-ERK levels in KGN cells with *PROCR* knockdown. One of three experiments was shown.

that Procr marks a subpopulation of GCs that have higher proliferative ability and may be in an immature/undifferentiated state.

Knockdown of *PROCR* inhibits AKT and ERK signaling pathway in granulosa cells

To gain molecular insights of the proliferative ability of Procr+ GCs, we inhibited *PROCR* expression by short haprpin RNAs (shRNAs) in KGN cells (a human ovarian GC-like tumor cell line). Knockdown of *PROCR* inhibited the proliferation as shown by decreased EdU staining (Figures 3A and 3B), as well as reduction in cell numbers (Figures 3C and 3D). Furthermore, knockdown of *PROCR* up-regulated the expression of *Cyp19a1*, *Esr2*, *Fshr*, and *Lhcgr* (Figure 3E), suggesting that the differentiation is skewed. Western analysis indicated the decreased phosphorylation of AKT and ERK upon *PROCR* knockdown (Figures 3F and S2). This is consistent with the known role of PI3K/Akt and MAPK signaling pathways in GC proliferation (Liu et al., 2020; Wu et al., 2019). Together, PROCR controlled PI3K/Akt and MAPK/Erk signaling pathways to regulate GCs and follicle development.

Procr+ cells contribute to granulosa cell expansion during follicle development

To investigate the contribution of Procr+ GCs during follicle development *in vivo*, we utilized a *Procr-Cre* knock-in line, with a Cre inserted after the fourth (last) exon of *Procr* gene (Q.C. Yu and Y.A. Zeng, unpublished data). Lineage tracing was performed using *Procr-Cre;R26-mTmG* mice (Figure S1B). Procr+ GCs and their progeny were labeled with mGFP expression, reflecting the contribution of Procr+ GCs in folliculogenesis (Figure 4A). Ovaries were harvested and the mGFP+ cells were analyzed by section imaging. In contrast to the decreased proportion of Procr+ cells along the follicle development (shown in Figure 1), the progeny of Procr+ cells increased while the follicle advances. We observed single mGFP+ cell in primordial follicles (Figure 4B), and 3∼4 mGFP+ cells in primary follicles (Figure 4C). In

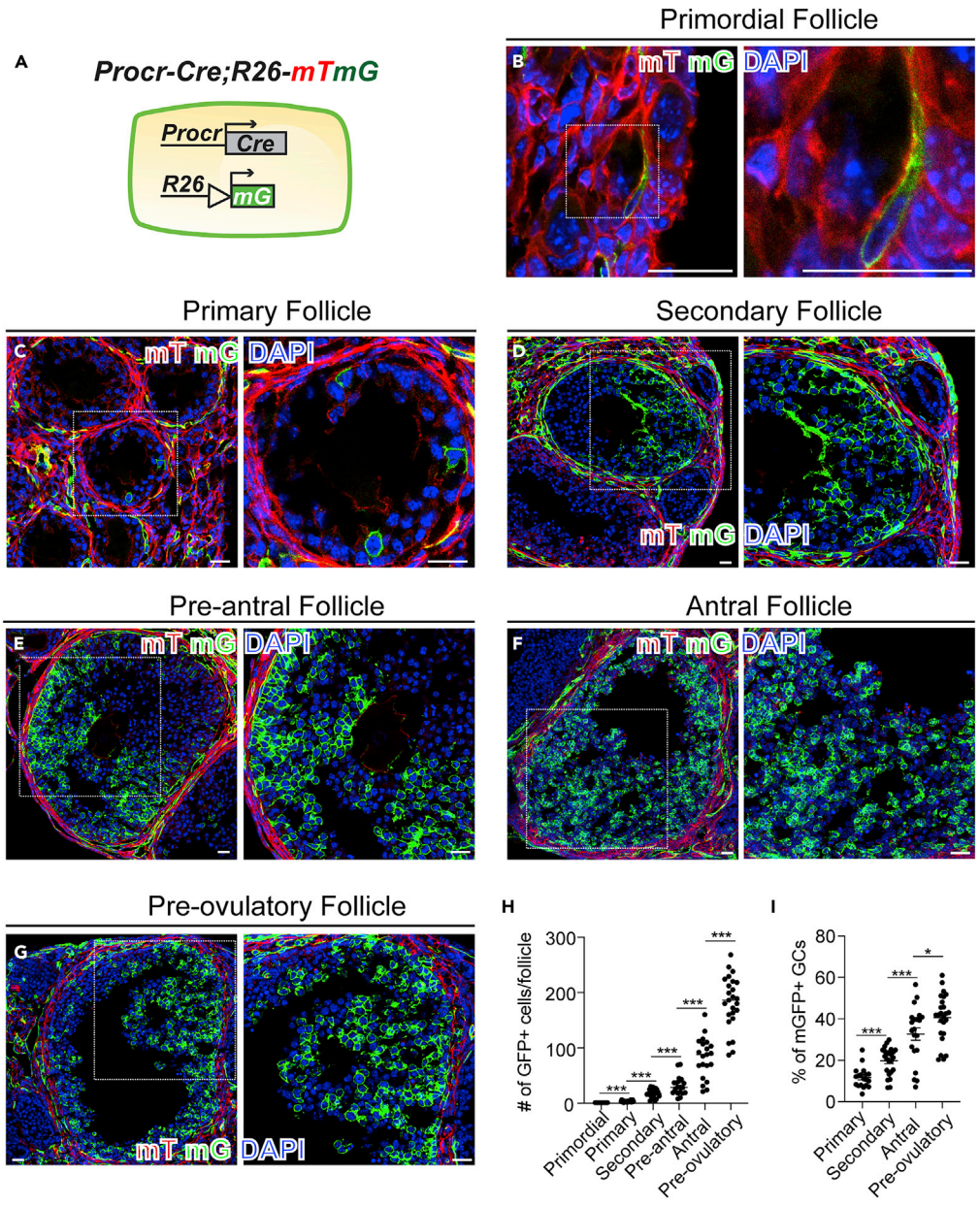

Figure 4. Procr+ cells contribute to granulosa cells' expansion

(A) Illustration of lineage tracing using *Procr-Cre;R26-mTmG* mice. Procr+ cells and their progeny were labeled by mGFP expression.

(B and C) Section imaging showing single mGFP+ GC in primordial follicles (B) and 3–4 mGFP+ GCs in primary follicle (C). Scale bars, 20 μm. n = 3 mice and representative image was shown.

(D–G) Section imaging showing the number of mGFP+ GCs expanded along follicular development, i.e., secondary (D), pre-antral (E), antral (F), and pre-ovulatory (G) follicles. Scale bar, 20 μm. n = 3 mice and representative image was shown.

(H and I) Quantification of mGFP+ GC numbers (H) and percentage of mGFP+ GCs (mGFP + GCs/all GCs) (I) of different stages per follicle exhibited the continuous expansion of mGFP+ GCs during tracing. At least 20 follicles in different stages of follicles from three mice were counted as the number of GFP+ cells per follicle. Unpaired two-tailed Student's t test is used for comparison. Data are presented as mean ± SEM. ***$p < 0.001$, *$p < 0.05$.

large follicles, including second, pre-antral, antral, and pre-ovulatory follicle, the number of mGFP+ GCs was dramatically increased (Figures 4D–4H). The proportion of mGFP+ GCs was also increased along follicle development (Figure 4I). The lineage tracing results validated the *in vivo* proliferative and

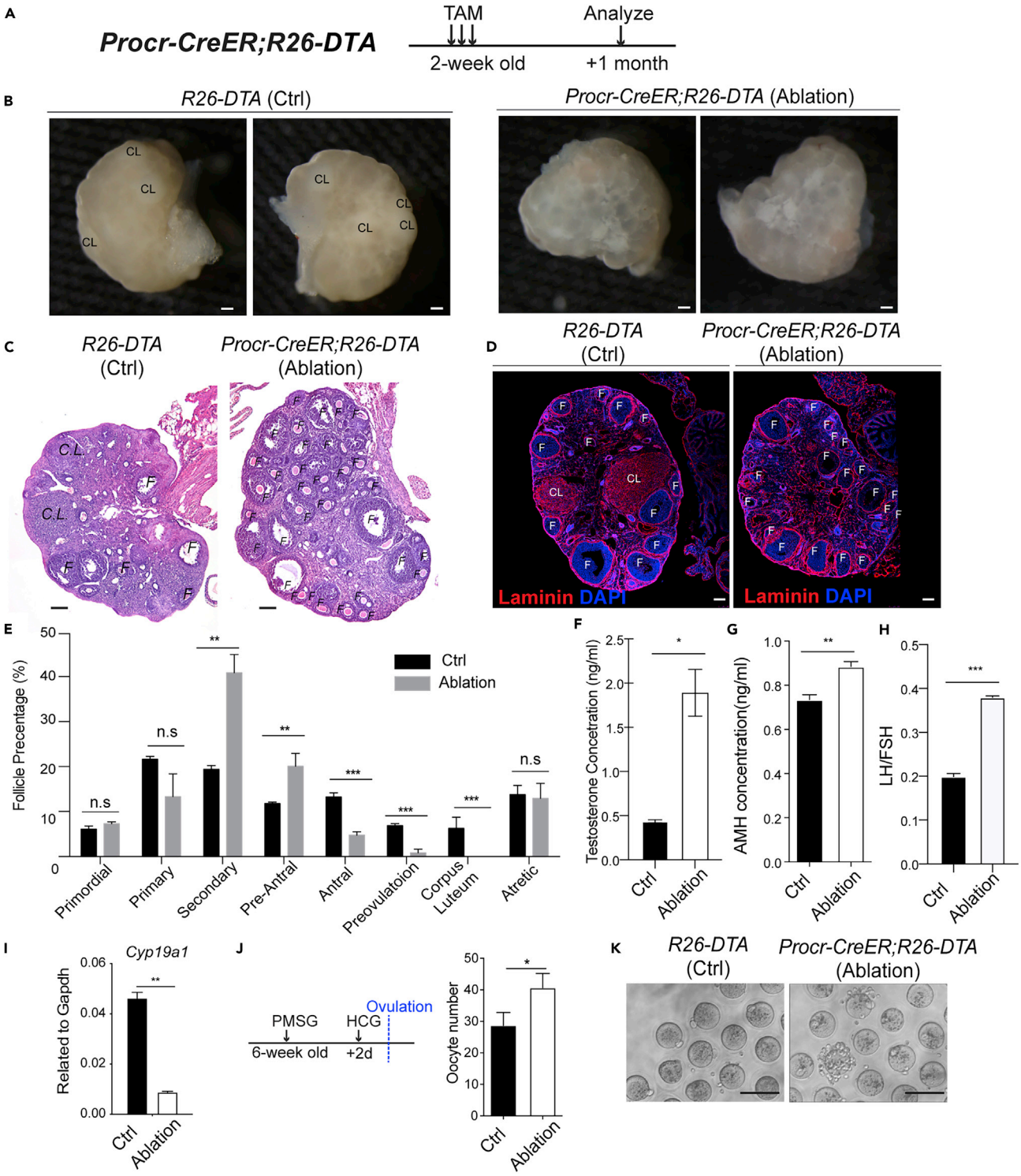

Figure 5. Ablation of Procr+ cells disrupts ovarian follicle development and leads to polycystic ovary syndrome phenotype

(A) Illustration of Procr+ cells ablation using *Procr-CreER;R26-DTA* mice. TAM was administered to 2-week-old mice, and the ovaries were analyzed at 1 month post injection.

(B–D) Whole-mount images (B), H&E section staining (C), and confocal section imaging (D) showing Procr+ cells ablation resulted in more immature follicles and less corpus luteum compared with control (Ctrl). Scale bars, 200 μm in (B) and 100 μm in (C and D). n = 3 mice in each experimental group, and representative image was shown.

Figure 5. *Continued*

(E) Quantification of the percentage of follicle in different stages. Data are presented as mean ± SEM. Unpaired two-tailed Student's t test is used for comparison. n = 3 mice in each experimental group. n.s, not significant. **p < 0.01. ***p < 0.001.

(F–H) Plasma testosterone (F), AMH (G) concentration, and LH/FSH ratio (H) in the serum of control and ablation mice. Data are presented as mean ± SEM. Unpaired two-tailed Student's t test is used for comparison. n = 3 mice in each experimental group. *p < 0.05, **p < 0.01, ***p < 0.001.

(I) qPCR analysis of *Cyp19a1* expression in the ovary of control and ablation mice. Data are presented as mean ± SEM. Unpaired two-tailed Student's t test is used for comparison. **p < 0.01.

(J) Illustration of superovulation strategy, and quantification of the number of ovulated oocytes from control and ablation mice. n = 3 mice in each experimental group. Data are presented as mean ± SEM. Unpaired two-tailed Student's t test is used for comparison. *p < 0.05.

(K) Representative images showed sticky granulosa cells to the oocytes and abnormal polar bodies in ablation mice after superovulation. Scale bars, 100 μm.

differentiation ability of Procr+ GCs and visualized their contribution to GC expansion during follicle development.

Ablation of Procr+ cells disrupts ovarian follicle development and leads to polycystic ovary syndrome phenotype

Next we investigated the significance of Procr+ GCs in folliculogenesis *in vivo*. We performed targeted ablation of Procr+ cells using *Procr-CreER;R26-DTA* mice (Figure S1C). Diphtheria toxin (DTA) was expressed to ablate Procr+ cells, and we examined its impact in follicle development. Two-week old mice were administered Tamoxifen (TAM) every other day for a total of three times, and the ovaries were examined after 1 month (Figure 5A). By whole-mount imaging, we observed fewer corpus luteum in the ablation group compared with the control (Figure 5B). By section imaging, the ablation group exhibited accumulation of small follicles and lack of corpus luteum (Figures 5C and 5D). Quantification revealed the increased percentage of immature follicles (secondary follicle, pre-antral follicle) and decreased proportion of mature follicles (antral follicle, pre-ovulatory follicle) in the ablation group compared with the control (Figure 5E). The lack of corpus luteum in the ablation group was a sign of anovulation (Figures 5C–5E). In addition, plasma testosterone, anti-Müllerian hormone (AMH) level, and luteinizing hormone (LH)/FSH ratio was significantly increased after ablation of Procr+ cells (Figures 5F–5H). qPCR analysis indicated the downregulation of *Cyp19a1* (Figure 5I). Upon PMSG/HCG-stimulated superovulation, the ablated group yielded more oocytes in numbers compared with the control (Figure 5J). The polar bodies in the ablation group also appeared abnormal (Figure 5K). Interestingly, in many cases, it appeared that GCs adhered to the surface of the oocytes (Figure 5K). These observations are reminiscent of the clinical features of PCOS. Together, targeted ablation of Procr+ cells suppressed follicle development and induced phenotypes of PCOS.

DISCUSSION

In this study, we identified a subpopulation of GCs that expressed Procr, exhibited higher proliferation compared with the rest GCs, and were important for follicle development. Knockdown of *PROCR* suppressed AKT and ERK signaling activities, rendering reduced proliferation and increased expression of differentiated genes in GCs. *In vivo*, Procr+ GCs contributed to increasing numbers of GCs shown by lineage tracing. Finally, targeted ablation of Procr+ cells disrupted ovarian follicle development, leading to PCOS phenotype.

The rapid proliferation of the GCs in the growing follicles as well as their exertion of various specialized functions have brought about the notion that the population of GCs in a single healthy follicle is heterogeneous, consisting of subpopulations of differentiated and less differentiated cells (Kossowska-Tomaszczuk et al., 2009). Several studies have reported that a subpopulation of GCs have proliferative capacity and can form colonies in culture (Lavranos TC et al., 1994; Rodgers HF et al., 1995); they can divide for at least 10 times to support follicle growth and oocyte maturation in the growing follicles (Hirshfield, 1991). Yet, little is known about such a subpopulation. In this study, our findings suggest that Procr+ GCs to some extend exhibit progenitor-like characteristics. They are highly proliferative and have lower expression of differentiation gene, e.g., *Cyp19a1*, *Fshr*, and *Lhcgr*.

The *in vivo* contribution and significance of Procr+ GCs during folliculogenesis was demonstrated by lineage tracing and targeted ablation experiments. Using *Procr-Cre;R26-mTmG* mouse model, we observed that the majority of GCs were derived from Procr+ cells during folliculogenesis. Upon targeted ablation of Procr+ cells using *Procr-CreER;R26-DTA* mouse model, the ovarian follicle development was disrupted, manifesting the PCOS phenotype. Ablation of Procr+ GCs led to accumulation of secondary and pre-antral follicles, and appearance of anovulation. It is worth noting that *Cyp19a1* was shown to be downregulated after Procr+ cells ablation, resulting in increase in plasma testosterone level. This may be because GCs in

early follicles do not express *Cyp19a1* (Stocco, 2008). These findings reveal an indispensable role of Procr+ GCs during follicle development.

Owing to the heterogeneity of PCOS, it has been challenging to establish a genetic animal model that displays the main characteristics of PCOS. Common PCOS models are induced models with chronic exposure to testosterone or the aromatase inhibitor letrozole (Kauffman et al., 2015; van Houten et al., 2012). In this study, we established a new PCOS mouse model, *Procr-CreER;R26-DTA*, by targeted ablation of Procr+ GCs. Our model recapitulates the clinical features of PCOS, such as hyperandrogenism, polycystic ovarian morphology, and chronic anovulation. The advantages brought by the new mouse model will be of broad value in studies of PCOS. Of note, the role of Procr goes beyond a surface marker. It plays functional roles in GCs proliferation. Knockdown of *PROCR* suppressed AKT and ERK signaling activities, rendering reduced proliferation and increased expression of differentiated genes in GCs. Future study may investigate the association of PROCR signaling pathway gene mutations with PCOS in human patients.

In conclusion, we reveal for the first time that Procr+ GCs plays a key role in ovarian follicle development by promoting proliferation and suppressing differentiation of GCs. Ablation of Procr+ cells disrupts ovarian follicle development and leads to a PCOS phenotype. Our findings not only shed new light on the role of Procr+ GCs in folliculogenesis but also extend knowledge of potential genes associated with PCOS in human patients.

Limitations of the study

The results of this study were obtained from mouse models. Further studies on human ovarian tissues would advance our understanding on the role of PROCR in follicle development and PCOS.

Resource availability

Lead contact

Professor Wen Li (liwen@smmu.edu.cn).

Materials availability

Requests for further information or materials should be directed to the lead contact.

Data and code availability

Requests for biological datasets should be directed to the lead contact.

METHODS

All methods can be found in the accompanying Transparent methods supplemental file.

SUPPLEMENTAL INFORMATION

Supplemental information can be found online at https://doi.org/10.1016/j.isci.2021.102065.

ACKNOWLEDGMENTS

This research was supported by grants from National Natural Science Foundation of China (81873821 and 82071605 to W.L.; 31625020, 31530045, 31830056, and 31861163006 to Y.A.Z.; 81570759 and 81270938 to J.F.), National Key Research and Development Program of China (2020YFA0509002, 2019YFA0802002 to Y.A.Z.; 2016YFC1305301 to J.F.), the Chinese Academy of Sciences (XDB19020200 and XDA16020200 to Y.A.Z.), Zhejiang Provincial Key Disciplines of Medicine (Innovation Discipline, 11-CX24 to J.F.), Fundamental Research Funds for the Central Universities (2020XZZX002-22 to J.F.), China Postdoctoral Science Foundation (2020TQ0260 to J.W.), and Zhejiang Provincial Preferential Postdoctoral Foundation (ZJ2020150 to J.W.).

AUTHOR CONTRIBUTIONS

W.L. and Y.A.Z. designed the project. J.W. performed lineage tracing, target ablation, primary cell culture, staining, and qPCR. K.C. performed RNA *in situ*, western blotting, KGN cell line culture, and staining. Y.W. performed superovulation and oocytes collection. J.F. and J.L. helped project design. J.W., K.C., W.L., and Y.A.Z. analyzed the data and wrote the manuscript.

DECLARATION OF INTERESTS

The authors declare no competing interests.

Received: September 27, 2020
Revised: November 20, 2020
Accepted: January 11, 2021
Published: February 19, 2021

REFERENCES

Azziz, R., Carmina, E., Chen, Z., Dunaif, A., Laven, J.S., Legro, R.S., Lizneva, D., Natterson-Horowtiz, B., Teede, H.J., and Yildiz, B.O. (2016). Polycystic ovary syndrome. Nat. Rev. Dis. Primers *2*, 16057.

Balazs, A.B., Fabian, A.J., Esmon, C.T., and Mulligan, R.C. (2006). Endothelial protein C receptor (CD201) explicitly identifies hematopoietic stem cells in murine bone marrow. Blood *107*, 2317–2321.

Cheng, T., Liu, D., Griffin, J.H., Fernandez, J.A., Castellino, F., Rosen, E.D., Fukudome, K., and Zlokovic, B.V. (2003). Activated protein C blocks p53-mediated apoptosis in ischemic human brain endothelium and is neuroprotective. Nat. Med. *9*, 338–342.

Eppig, J.J. (2001). Oocyte control of ovarian follicular development and function in mammals. Reproduction *122*, 829–838.

Fukudome, K., and Esmon, C.T. (1994). Identification, cloning, and regulationof a novel endothelial cell protein C/activated ProteinC receptor. J. Biol. Chem. *269*, 26486–26491.

Fan, H.Y., Liu, Z., Cahill, N., and Richards, J.S. (2008). Targeted disruption of Pten in ovarian granulosa cells enhances ovulation and extends the life span of luteal cells. Mol. Endocrinol. *22*, 2128–2140.

Gramling, M.W., Beaulieu, L.M., and Church, F.C. (2010). Activated protein C enhances cell motility of endothelial cells and MDA-MB-231 breast cancer cells by intracellular signal transduction. Exp. Cell Res. *316*, 314–328.

Hirshfield, A.N. (1991). Development of follicles in the mammalian ovary. Int. Rev. Cytol. *124*, 43–101.

van Houten, E.L., Kramer, P., McLuskey, A., Karels, B., Themmen, A.P., and Visser, J.A. (2012). Reproductive and metabolic phenotype of a mouse model of PCOS. Endocrinology *153*, 2861–2869.

Kauffman, A.S., Thackray, V.G., Ryan, G.E., Tolson, K.P., Glidewell-Kenney, C.A., Semaan, S.J., Poling, M.C., Iwata, N., Breen, K.M., Duleba, A.J., et al. (2015). A novel letrozole model recapitulates both the reproductive and metabolic phenotypes of polycystic ovary syndrome in female mice. Biol. Reprod. *93*, 69.

Kipp, J.L., Kilen, S.M., Woodruff, T.K., and Mayo, K.E. (2007). Activin regulates estrogen receptor gene expression in the mouse ovary. J. Biol. Chem. *282*, 36755–36765.

Kossowska-Tomaszczuk, K., De Geyter, C., De Geyter, M., Martin, I., Holzgreve, W., Scherberich, A., and Zhang, H. (2009). The multipotency of luteinizing granulosa cells collected from mature ovarian follicles. Stem Cells *27*, 210–219.

Lavranos TC, R.H., Bertoncello, I., and Rodgers, R.J. (1994). Anchorage-independent culture of bovine granulosa cells: the effects of basic fibroblast growth factor and dibutyryl cAMP on cell division and differentiation. Exp. Cell Res. *211*, 245–251.

Liu, C., Peng, J., Matzuk, M.M., and Yao, H.H. (2015). Lineage specification of ovarian theca cells requires multicellular interactions via oocyte and granulosa cells. Nat. Commun. *6*, 6934.

Liu, M., Qiu, Y., Xue, Z., Wu, R., Li, J., Niu, X., Yuan, J., Wang, Y., and Wu, Q. (2020). Small extracellular vesicles derived from embryonic stem cells restore ovarian function of premature ovarian failure through PI3K/AKT signaling pathway. Stem Cell Res. Ther. *11*, 3.

Lu, C. (2005). Granulosa cell proliferation differentiation and its role in follicular development. Chin. Sci. Bull. *50*, 2665.

Parvari, S., Yazdekhasti, H., Rajabi, Z., Gerayeli Malek, V., Rastegar, T., and Abbasi, M. (2016). Differentiation of mouse ovarian stem cells toward oocyte-like structure by coculture with granulosa cells. Cell. Reprogram. *18*, 419–428.

Pisarska, M.D., Bae, J., Klein, C., and Hsueh, A.J. (2004). Forkhead l2 is expressed in the ovary and represses the promoter activity of the steroidogenic acute regulatory gene. Endocrinology *145*, 3424–3433.

Richards, J.S., and Pangas, S.A. (2010). The ovary: basic biology and clinical implications. J. Clin. Invest. *120*, 963–972.

Rodgers HF, L.T., Vella, C.A., and Rodgers, R.J. (1995). Basal lamina and other extracellular matrix produced by bovine granulosa cells in anchorage-independent culture. Cell Tissue Res. *282*, 463–471.

Rotterdam ESHRE/ASRM-Sponsored PCOS consensus workshop group (2004). Revised 2003 consensus on diagnostic criteria and long-term health risks related to polycystic ovary syndrome (PCOS). Hum. Reprod. *19*, 41–47.

Da Silva-Buttkus, P., Jayasooriya, G.S., Mora, J.M., Mobberley, M., Ryder, T.A., Baithun, M., Stark, J., Franks, S., and Hardy, K. (2008). Effect of cell shape and packing density on granulosa cell proliferation and formation of multiple layers during early follicle development in the ovary. J. Cell Sci. *121*, 3890–3900.

Stocco, C. (2008). Aromatase expression in the ovary: hormonal and molecular regulation. Steroids *73*, 473–487.

Stocco, C., Telleria, C., and Gibori, G. (2007). The molecular control of corpus luteum formation, function, and regression. Endocr. Rev. *28*, 117–149.

Su, Y.Q., Wu, X., O'Brien, M.J., Pendola, F.L., Denegre, J.N., Matzuk, M.M., and Eppig, J.J. (2004). Synergistic roles of BMP15 and GDF9 in the development and function of the oocyte-cumulus cell complex in mice: genetic evidence for an oocyte-granulosa cell regulatory loop. Dev. Biol. *276*, 64–73.

Uda, M., Ottolenghi, C., Crisponi, L., Garcia, J.E., Deiana, M., Kimber, W., Forabosco, A., Cao, A., Schlessinger, D., and Pilia, G. (2004). Foxl2 disruption causes mouse ovarian failure by pervasive blockage of follicle development. Hum. Mol. Genet. *13*, 1171–1181.

Wang, H.X., Li, T.Y., and Kidder, G.M. (2010). WNT2 regulates DNA synthesis in mouse granulosa cells through beta-catenin. Biol. Reprod. *82*, 865–875.

Wang, D., Cai, C., Dong, X., Yu, Q.C., Zhang, X.O., Yang, L., and Zeng, Y.A. (2015a). Identification of multipotent mammary stem cells by protein C receptor expression. Nature *517*, 81–84.

Wang, Y., Liu, W., Du, J., Yu, Y., Liang, N., Liang, M., Yao, G., Cui, S., Huang, H., and Sun, F. (2015b). NGF promotes mouse granulosa cell proliferation by inhibiting ESR2 mediated down-regulation of CDKN1A. Mol. Cell. Endocrinol. *406*, 68–77.

Wang, D., Liu, C., Wang, J., Jia, Y., Hu, X., Jiang, H., Shao, Z.M., and Zeng, Y.A. (2018). Protein C receptor stimulates multiple signaling pathways in breast cancer cells. J. Biol. Chem. *293*, 1413–1424.

Wang, J., Wang, D., Chu, K., Li, W., and Zeng, Y.A. (2019). Procr-expressing progenitor cells are responsible for murine ovulatory rupture repair of ovarian surface epithelium. Nat. Commun. *10*, 4966.

Wang, D., Wang, J., Bai, L., Pan, H., Feng, H., Clevers, H., and Zeng, Y.A. (2020). Long-Term expansion of pancreatic islet organoids from resident Procr(+) progenitors. Cell *180*, 1198–1211.e19.

Wu, Y., Xiao, H., Pi, J., Zhang, H., Pan, A., Pu, Y., Liang, Z., Shen, J., and Du, J. (2019). EGFR promotes the proliferation of quail follicular granulosa cells through the MAPK/extracellular

signal-regulated kinase (ERK) signaling pathway. Cell Cycle *18*, 2742–2756.

Yu, F.Q., Han, C.-S., Yang, W., Jin, X., Hu, Z.Y., and Liu, Y.X. (2005). Role of erk1/2 in fsh-induced pcna expression and steroidogenesis in granulosa cells. Front. Biosci. *10*, 896–904.

Yu, Q.C., Song, W., Wang, D., and Zeng, Y.A. (2016). Identification of blood vascular endothelial stem cells by the expression of protein C receptor. Cell Res. *26*, 1079–1098.

Zhang, H., and Liu, K. (2015). Cellular and molecular regulation of the activation of mammalian primordial follicles: somatic cells initiate follicle activation in adulthood. Hum. Reprod. Update *21*, 779–786.

Zhang, H., Risal, S., Gorre, N., Busayavalasa, K., Li, X., Shen, Y., Bosbach, B., Brännström, M., and Liu, K. (2014). Somatic cells initiate primordial follicle activation and govern the development of dormant oocytes in mice. Curr. Biol. *24*, 2501–2508.

Zhang, Y., Yan, Z., Qin, Q., Nisenblat, V., Chang, H.M., Yu, Y., Wang, T., Lu, C., Yang, M., Yang, S., et al. (2018). Transcriptome landscape of human folliculogenesis reveals oocyte and granulosa cell interactions. Mol. Cell *72*, 1021–1034.e4.

iScience, Volume *24*

Supplemental Information

Procr-expressing granulosa cells are highly proliferative and are important for follicle development

Jingqiang Wang, Kun Chu, Yinghua Wang, Jinsong Li, Junfen Fu, Yi Arial Zeng, and Wen Li

Figure S1, Illustration of mouse models used, Related to Figure 1, Figure 4 and Figure 5.

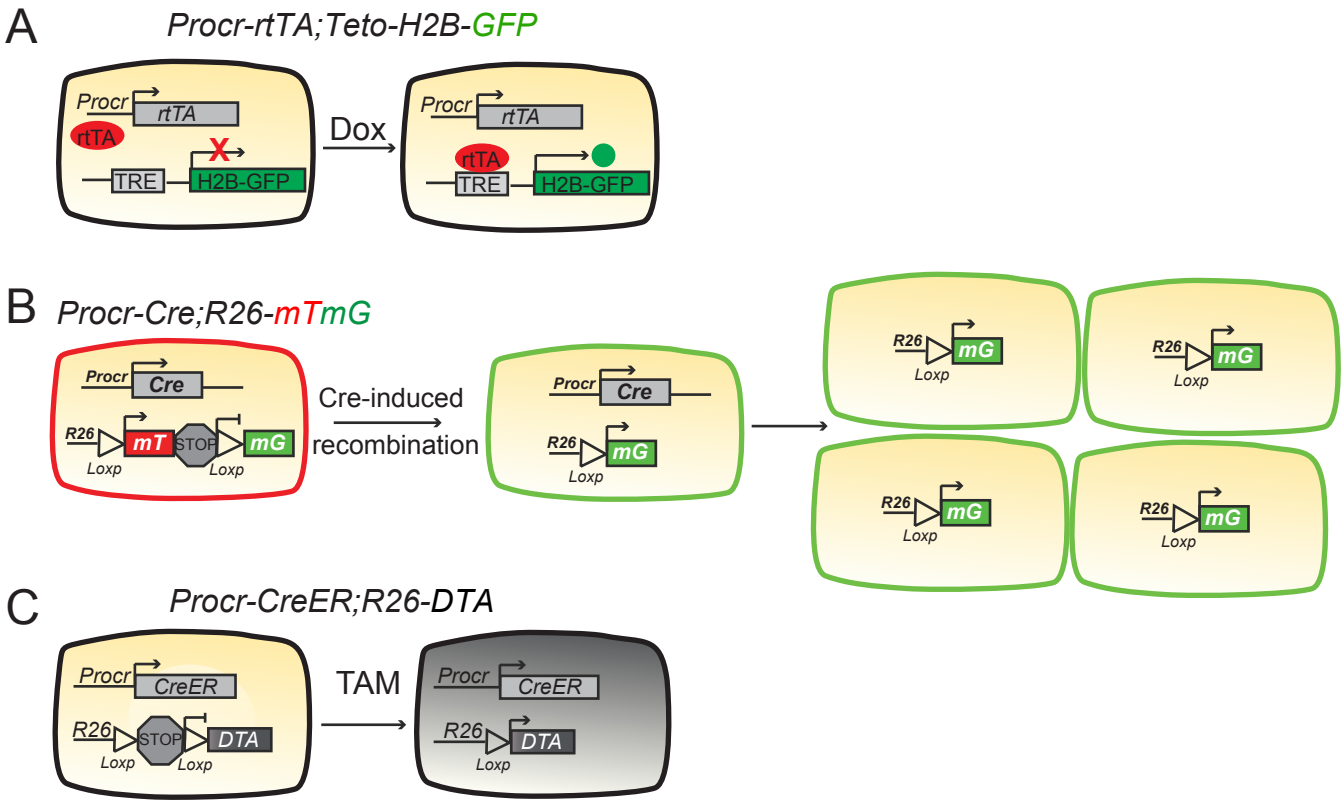

(A) Illustration of the Procr+ cell reporter, *Procr-rtTA;TetO-H2B-GFP* mouse. rtTA is specifically expressed in Procr+ cells, while H2B-GFP expression is under transcriptional control of a tetracycline-responsive promoter element (TRE). In the absence of doxycycline (DOX), rtTA cannot combine to TRE. In the presence of DOX, rtTA binds to TRE and induce H2B-GFP expression specifically in Procr+ cells. Related to Figure 1.

(B) Illustration of lineage tracing using *Procr-Cre;R26-mTmG* mouse. Initially, all cells express membrane Tomato (mT) driven by a ubiquitous Rosa26 promoter (R26). Cre is expressed in the Procr+ cells driven by the Procr promoter. Cre induces the recombination of the two Loxp sites, resulting in the removal of mT and STOP cassettes, allowing the expression of membrane GFP (mGFP). The DNA recombination is irreversible, the expression of mG is no longer depend on Procr-driven Cre, hence while Procr+ cell divides, all it's progeny express mGFP. Related to Figure 4.

(C) Illustration of the ablation of Procr+ cells using *Procr-CreER;R26-DTA* mouse. CreER is specifically expressed in Procr+ cells, while Diphtheria toxin A (DTA) expression is driven by R26 but is blocked by a stop cassette. Upon tamoxifen (TAM) administration, in Procr+ cells, Cre mediated DNA recombination cleaves the stop cassette and allow DAT expression. Hence Procr+ cells are targeted ablated by DTA. Related to Figure 5.

Figure S2, Whole blots of related proteins, Related to Fig 3F.

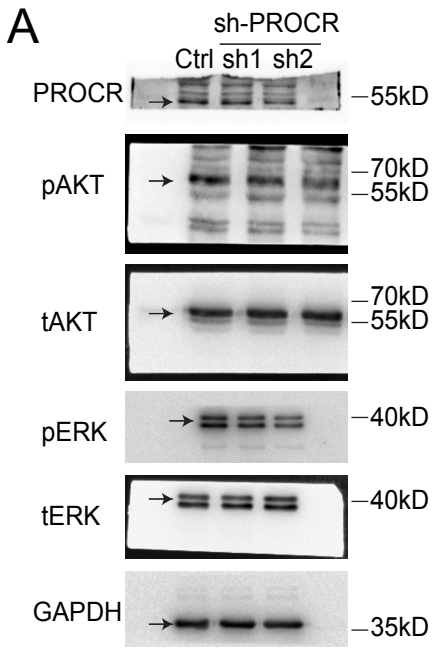

(A) Whole blots showing decreased p-AKT and p-ERK levels in KGN cells with PROCR knockdown. One of three experiments was shown.

Transparent Methods

Experiment animals

TetO-H2B-GFP (JAX: 005104), *R26-mTmG* (JAX: 007676), *R26-DTA* (JAX:010527), *Procr-CreER* (JAX: 033052), *Procr-rtTA (*Wang et al., 2019*)*, *Procr-Cre* (unpublished*,* Yu and Zeng) and C57BL/6J mice were used in this study. The following lines were used for in vivo genetic lineage tracing or targeted ablation (illustrated in Figure S1): *Procr-rtTA;TetO-H2B-GFP* (Dox inducible Procr+ cell reporter), *Procr-CreER;R26-DTA* (Ablation of Procr+ cells by DTA), *Procr-Cre;R26-mTmG* (Lineage tracing of Procr+ cells with *Procr-Cre*). For targeted ablation experiment, three intraperitoneal injection of tamoxifen (TAM, Sigma- Aldrich, catalog #T5648, 2mg/25g body weight, on every second day) was performed in 2-week-old *Procr-CreER;R26-DTA* mice and the mice were sacrificed one month later. The mice were in natural estrus cycle if not specified, and the ovaries were harvested in diestrus stage. For visualize the localization and expression pattern of Procr+ GCs, we generated *Procr-rtTA;tetO-H2B-GFP* mice and Dox hyclate (Sigma, catalog #D9891) was added to drinking water of postnatal day 10 mice at a concentration of 1mg/ml for 2 days to induce stable expression of histone 2B-GFP protein in Procr+ cells. All animal protocols (IBCB0065) were approved by the Animal Care and Use Committee of Shanghai Institute of Biochemistry and Cell Biology, Chinese Academy of Sciences.

In situ hybridization of *Procr*

Mouse ovaries were fixed overnight in neutral formalin at room temperature, dehydrated in graded ethanol and paraffin embedded. Serial sections (5 μm) were prepared for *in situ* hybridization of *Procr*. RNA *in situ* was conducted using RNA scope kit (Advanced Cell Diagnostics) based on the manufacturer's instructions (REF#410321).

Tissue processing and follicle counting

For follicle counting, serial paraffin sections (5 μm) were prepared and every fifth slice was stained by hematoxylin & eosin. Counting was conducted by operators' double-blinded to either treatment condition or control group. Follicles were counted in every fifth slice to avoid repetitive counting.

Primordial follicles were defined as an oocyte surrounded by a single layer of flattened GCs or both flattened and cuboidal GCs. Primary follicles were defined as an oocyte completed surrounded by a single layer of cuboidal GCs. Secondary follicles contained a larger oocyte and more than one layer of GCs, with no visible antrum. Pre-antral follicles were counted when follicles had emerging antral spaces, whilst antral follicles were counted when a clearly defined antrum appeared. Pre-ovulatory follicles were the largest follicular type with a cumulus granulosa cell layer. Atretic follicles were counted when the oocytes were of degenerate appearance or fragmenting (Mao et al., 2018; Myers et al., 2004).

Superovulation and oocytes collection

Mice were super-ovulated by the intraperitoneal injection of 10 IU of pregnant mare's serum gonadotropin (PMSG), followed by 10 IU human chorionic gonadotropin (hCG) 48 hours later. Approximately 16 hours after hCG injection, ampulla of oviducts were torn under a stereoscopic microscope, and cumulus-oocyte complexes were collected.

GC isolation, culture, and flow cytometry

Ovaries from 4-week old *R26-mTmG* mice were harvested, washed in cold PBS, and separated from ovarian bursa by microdissection under a stereomicroscope. Single cells were obtained following the protocol we described before (Wang et al., 2019). In general, minced ovarian pieces were digested with digest buffer (RPMI 1640 (Thermo Fisher, catalog #12633-012) with 5% fetal bovine serum (FBS, Hyclone), 1% penicillin–streptomycin (Thermo Fisher, catalog #15140122), 25 mM HEPES and 300U/ml collagenase IV (Worthington, catalog # LS004189)) at 37°C, 100 rpm for 1 hour, lysed with red blood cell lysis buffer (Sigma, catalog #R7757) , and then treated with 0.05%Trypsin-EDTA (Thermo Fisher, catalog # 25200056) and DNaseI (Sigma, catalog #D4263) before filtering through 70 μm cell strainers. For flow cytometry, ovarian cells were incubated on ice for 30 min with 1:200 Procr-Biotin antibody (Thermo Fisher, Cat#12-2012-82) and then incubated with Streptavidin-V450(BD, Cat# 560797). FACSJazz (Becton Dickinson) was

used for analysis and sorting. When analyzing the dissociated *R26-mTmG* ovarian cells by FACS contour plot with Tomato color on the X axis, the cells appeared as two populations (with two centers). We divided the two populations following the contour lines, and gated the left population as "mTom-low" (dimmer fluorescence) the right one as "mTom-high". The purity of sorted population was routinely checked and ensured to be >95%. For cell culture, GCs were resuspended in the fresh DMEM/F12 medium (Thermo Fisher, Cat#11320) containing 10% FBS (Hyclone), insulin-transferrin-selenium (Thermo Fisher, Cat#41440), EGF (BD, Cat#354001), 1% penicillin and streptomycin (Thermo Fisher, Cat#15140-122).

EdU staining

The proliferation of GCs in vitro was measured by 5-ethynyl-2-deoxyuridine (EdU) uptake following the manufacturer's instructions (Click-iT EdU Imaging Kit, Thermo Fisher, C10632). In brief, cultured cells were incubated with EdU for 1 hour. Cultured cells were fixed with PFA for 10 min following by wash with 3% BSA twice and pre-treated with 0.5% Triton-X 100 for 30 min, then incubated with the reagents in the Kit.

Immunohistochemistry

Ovaries were fixed in cold PFA for 2 hours, washed with PBS for three times and embedded with OCT (Thermo Fisher, Cat#D6506). 14 μm tissue sections were incubated in 0.1% Triton-X 100 diluted with PBS (PBST) for 20 min and blocked using 10% of FBS in PBST for 1 hour. Then sections were incubated with primary antibodies at 4 °C overnight, followed by incubated with secondary antibodies for 2 hours at room temperature, and counterstained with DAPI (Thermo Fisher, catalog #D3571). At least three times repeats were done per tissue block. Only representative images were shown. Confocal section images were captured using Leica DM6000 TCS/SP8 laser confocal scanning microscope.

Western Blotting

Cultured cells were directly lysed in SDS-PAGE loading buffer (100 mM Tris-HCl, 4% SDS, 20% glycerol, 2% mercaptoethanol, 0.1% bromophenol blue, pH 6.8) and boiled for 10min. Proteins were separated by SDS-PAGE and transferred to nitrocellulose membrane (GE company). Bolts were blocked with 3% BSA in TBST (50 mM Tris-HCl, 150 mM NaCl, 0.05% Tween-20, pH 7.5) for 1hr and incubated with primary antibodies at 4 °C overnight, followed by incubated with secondary IgG-HRP antibodies for 2 hours at room temperature. Protein bands were visualized with chemiluminescent reagent and exposed to Mini Chemiluminescent Imager. Image J was used to quantify the level of pAKT and pERK, and normalized to scramble control.

RNA isolation and qPCR

Total RNA was isolated from cells with Trizol (Thermo Fisher, catalog #15596018) according to the manufacturer's instructions. The cDNA was generated using the SuperScriptIII kit (Thermo Fisher, catalog #18080093). qPCR was carried out on a StepOne Plus (Applied Biosystems) with Power SYBR Green PCR Master Mix. RNA level was normalized to *Gapdh*. The primers used were:

Ms-Procr-F, CTCTCTGGGAAAACTCCTGACA;

Ms-Procr-R, CAGGGAGCAGCTAACAGTGA;

Ms-Cyp19a1-F, ATGTTCTTGGAAATGCTGAACCC;

Ms-Cyp19a1-R, AGGACCTGGTATTGAAGACGAG;

Ms-Foxl2-F, AAGTACCTGCAATCGGGGTTC;

Ms-Foxl2-R, GTTGTAGGAGTTCACGACGCC;

Ms-Fshr-F, CCTTGCTCCTGGTCTCCTTG;

Ms-Fshr-R, CTCGGTCACCTTGCTATCTTG;

Ms-Lhcgr-F, CGCCCGACTATCTCTCACCTA;

Ms-Lhcgr-R, GACAGATTGAGGAGGTTGTCAAA;

Ms-Esr1-F, TCCAGCAGTAACGAGAAAGGA;

Ms-Esr1-R, AGCCAGAGGCATAGTCATTGC;

Ms-Esr2-F, CTGTGATGAACTACAGTGTTCCC;

Ms-Esr2-R, CACATTTGGGCTTGCAGTCTG.

Antibodies

Antibodies used in immunohistochemistry were rabbit anti-Laminin (1:500, Sigma, catalog #L9393, RRID:AB_477163).

Antibodies used in Western blotting were rabbit anti-human PROCR (1:200, Novus, catalog #H00010544-D01P, RRID:AB_1579200), rabbit anti-human phospho-ERK (1:1000, Cell Signaling Technology, catalog #4370, RRID:AB_2315112), rabbit anti-human total ERK (1:100, Santa Cruz, catalog #sc-94, RRID:AB_2140110), rabbit anti-human phospho-Akt (1:1000, Cell Signaling Technology, catalog #9271, RRID:AB_329825), rabbit anti-human total Akt (1:1000, Cell Signaling Technology, catalog #4691, RRID:AB_915783), rabbit anti-human GAPDH (1:5000, Proteintech, catalog # 10494-1-AP, RRID:AB_2263076).

ELISA

Mouse Testosterone ELISA Kit, AMH ELISA Kit, FSH ELISA Kit and LH ELISA Kit were used to detect hormone level in mice serum following manufacturer's instructions. The absorbance was recorded at 450 nm and three samples from each group were tested.

Lentiviral production and GC infection

The shRNA targeting *PROCR* sequences were constructed as we previously described(Wang et al., 2018), and lentiviruses were produced in 293T cells by co-transfecting of the transfer vectors. The transfection was performed by Opti-MEM (Thermo Fisher, Cat#31985070), and the transfection media were replaced 12 hours post-transfection. Viral supernatants were collected at 48 hours with 0.45 μm membrane filtration. For GC infection, packaged virus was

diluted in the GC culture medium along with 1:100 polybrene (Sigma, Cat#TE-1003) for 12 hours and the infected GCs were harvested after 3 days.

Statistical analysis

All experiments were repeated at least 3 times (Details in the Figure legends). In Figure 4, we selected different stage of follicles and counted the number of GFP+ granulosa cells and total granulosa cells per follicle. At least 20 follicles were counted per stage. All analyses were performed with GraphPad PRISM 6 Prism (two-tailed Student's *t* tests or one-way analysis of variance). All the P values were calculated with the following significance: n.s. $P > 0.05$; * $P < 0.05$; ** $P < 0.01$; *** $P < 0.001$. Error bars represent the standard error of measurement (SEM).

Supplemental References

Mao, Z., Yang, L., Lu, X., Tan, A., Wang, Y., Ding, F., Xiao, L., Qi, X., and Yu, Y. (2018). C1QTNF3 in the murine ovary and its function in folliculogenesis. *Reproduction* (Cambridge, England) 155, 333-346.

Myers, M., Britt, K.L., Wreford, N.G., Ebling, F.J., and Kerr, J.B. (2004). Methods for quantifying follicular numbers within the mouse ovary. *Reproduction* (Cambridge, England) 127, 569-580.

Wang, D., Liu, C., Wang, J., Jia, Y., Hu, X., Jiang, H., Shao, Z.M., and Zeng, Y.A. (2018). Protein C receptor stimulates multiple signaling pathways in breast cancer cells. *The Journal of biological chemistry* 293, 1413-1424.

Wang, J., Wang, D., Chu, K., Li, W., and Zeng, Y.A. (2019). Procr-expressing progenitor cells are responsible for murine ovulatory rupture repair of ovarian surface epithelium. *Nature communications* 10.